Supporting Information

From layer sliding to near-zero compressibility: novel high-pressure flexibility and CO_2 site evolution in pre-ELM-11 and ELM-11

Jingyan Liu[1], Julia M. Barker[1], Jiabin Xu[1], Yining Huang[1]*, and Yang Song[1]*

[1] Department of Chemistry, University of Western Ontario, London, ON, N6A 5B7, Canada

*Corresponding author. Email: yhuang@uwo.ca; yang.song@uwo.ca

Section S1. Structural description of pre-ELM-11 and ELM-11

Pre-ELM-11 contains two crystallographically distinct 4,4′-bipyridine (bpy) species that play different structural roles (Fig. S1a,b). One bpy ligand coordinates directly to octahedral Cu(II) centers to form one-dimensional chains along the crystallographic b axis, whereas the second bpy is non-coordinated and links neighbouring Cu centers via hydrogen bonding to coordinated water molecules (O–H···N), generating 2D grid-like layers with cavities. The layers are offset and stacked, with Cu atoms positioned near the centres of cavities in adjacent layers. BF_4^- anions protrude into neighbouring cavities and participate in interlayer hydrogen bonding (O–H···F) with the structural water molecules; alternating parallel π–π stacking of bpy along the c axis further reinforces this arrangement, producing a densely packed structure without permanent microporosity. Upon dehydration, ELM-11 forms with all bpy ligands coordinated to Cu(II), yielding quasi-square 2D grid layers (Fig. S1c,d); the loss of interlayer hydrogen bonding is expected to increase interlayer compliance.

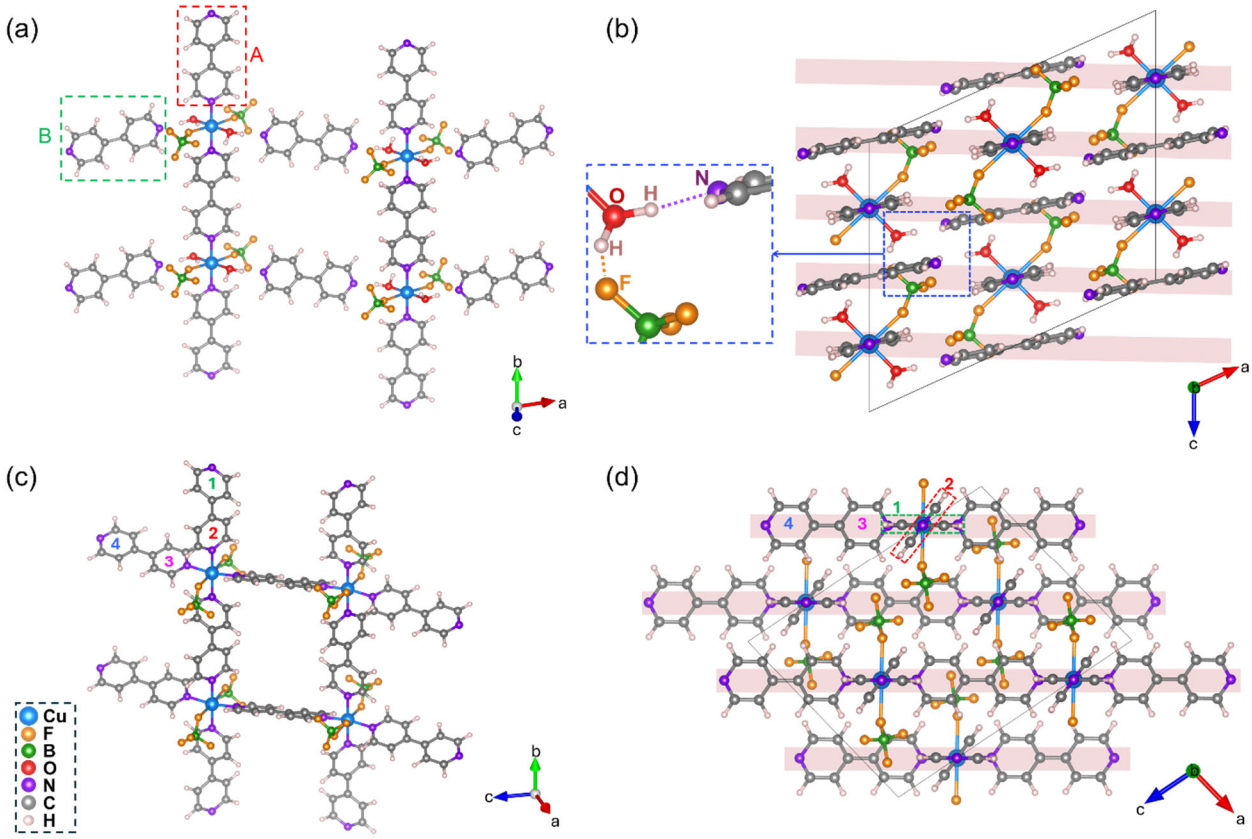

Fig. S1 Crystal structures of pre-ELM-11 and ELM-11: (a) a single 2D layer of pre-ELM-11 and (b) stacked layers viewed along the ac plane (insets highlight hydrogen bonding), together with the corresponding structures of ELM-11 ((c) single layer and (d) stacked layers) [1, 2]. Colour code: Cu (blue), F (orange), B (green), O (red), N (purple), C (grey), H (light pink). Pink rectangles in (b) and (d) outline a single layer.

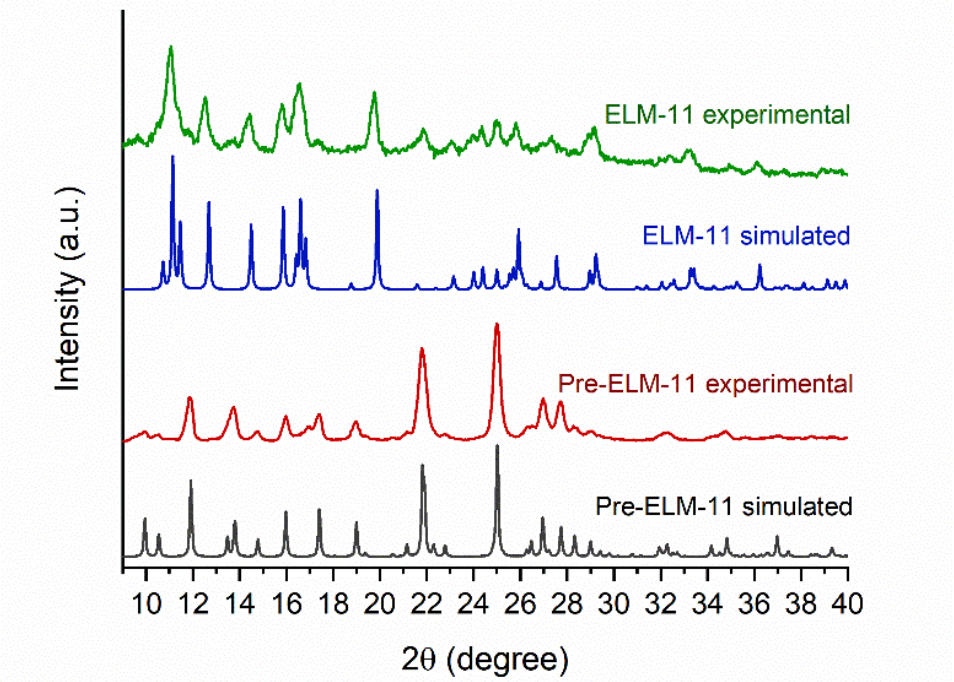

Fig. S2 Powder X-ray diffraction (PXRD) patterns of pre-ELM-11 and ELM-11 collected at the local laboratory (Cu Kα radiation, λ = 1.5406 Å), compared with the simulated patterns [1, 2].

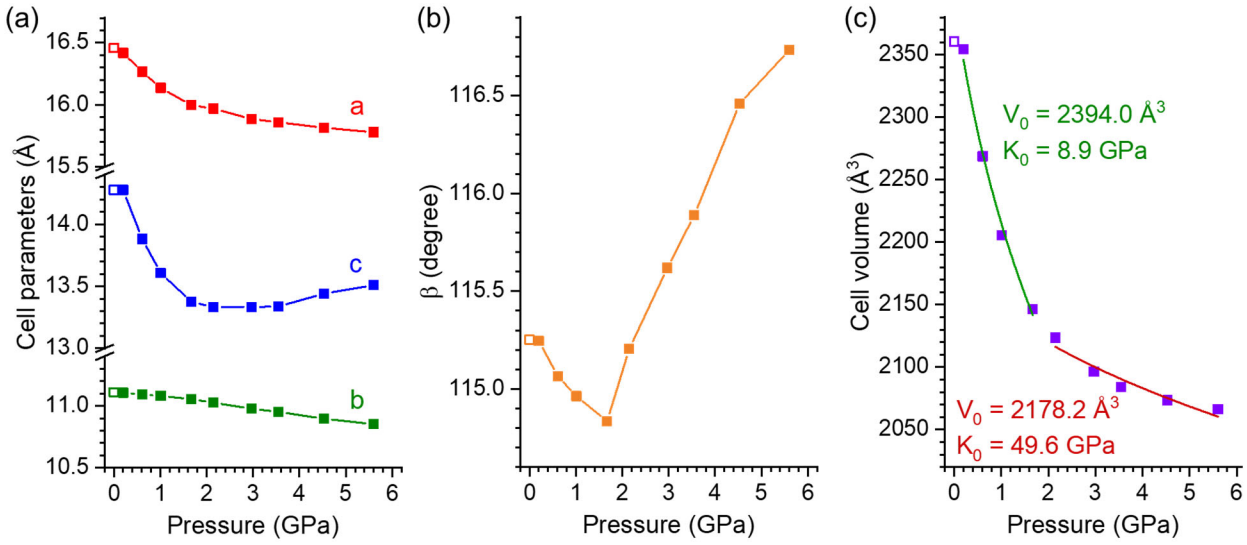

Fig. S3 Pressure dependence of (a) unit-cell parameters, (b) monoclinic angle β, and (c) unit-cell volume of pre-ELM-11 derived from Le Bail refinement of in situ synchrotron PXRD patterns collected over 0.20–5.60 GPa. Filled squares denote compression and open squares denote recovered data after pressure release.

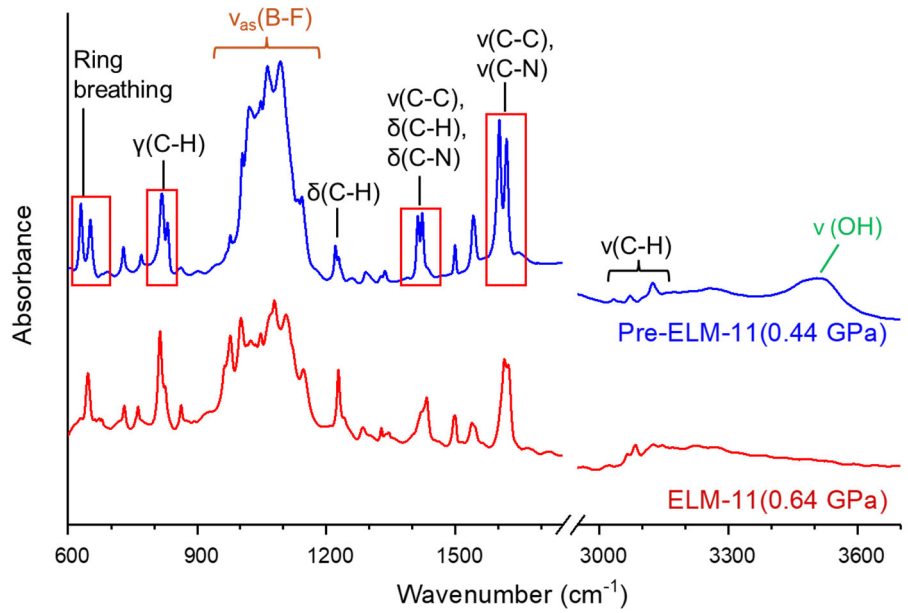

Fig. S4 In situ FTIR spectra of pre-ELM-11 (0.44 GPa) and ELM-11 (0.64 GPa) in the 600–3700 cm^{-1} range; the 1750–2950 cm^{-1} region is omitted for clarity.

Table S1 Assignments of the IR modes for pre-ELM-11 and ELM-11.

Experimental values (cm^{-1})		**Reference values (cm^{-1})**		**Assignments**	**Bond locations**
Pre-ELM-11 (0.50 GPa)	**ELM-11 (0.64 GPa)**	**Pre-ELM-11** [3]	**Free bpy** [4]		
629, 651	646		628	Ring breathing	bpy
817, 831	814	814, 829	831	γ(C-H)	bpy
960-1150	940-1170	950-1100	/	ν_{as}(B-F)	BF_4^-
1221, 1229	1228	1219, 1227	1238	δ(C-H)	bpy
1412, 1423	1433	1410, 1421	1449	ν(C-C), δ(C-H), δ(C-N)	bpy
1602, 1619	1617	1599, 1616	1606	ν(C-C), ν(C-N)	bpy
3025-3145	3050-3160			ν(C-H)	bpy
3508	/	3489	/	ν(O-H)	Structural H_2O
ν, stretching; γ, out of plane bending; δ, in plane bending; ρ, rocking; ω, wagging; s, symmetric.					

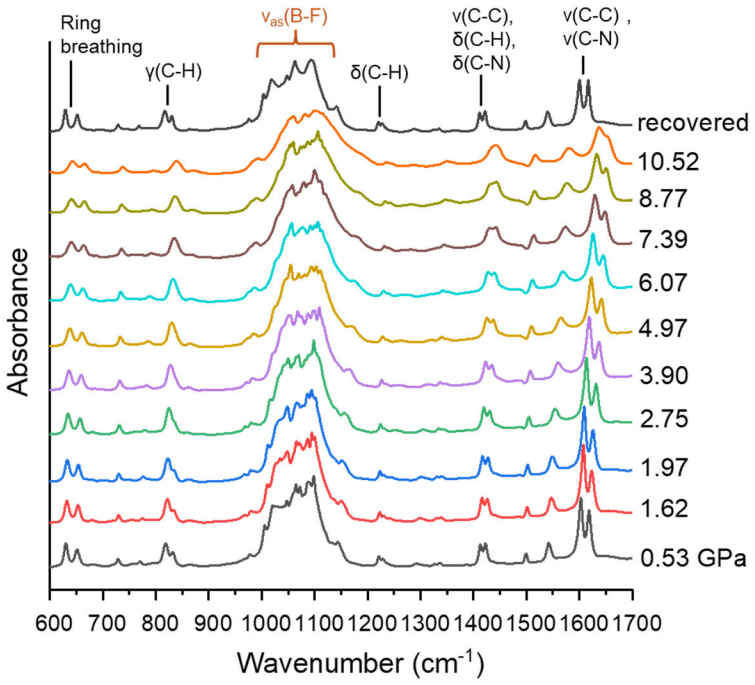

Fig. S5 Selected in situ FTIR spectra of pre-ELM-11 collected on compression and decompression in the 600–1700 cm^{-1} range.

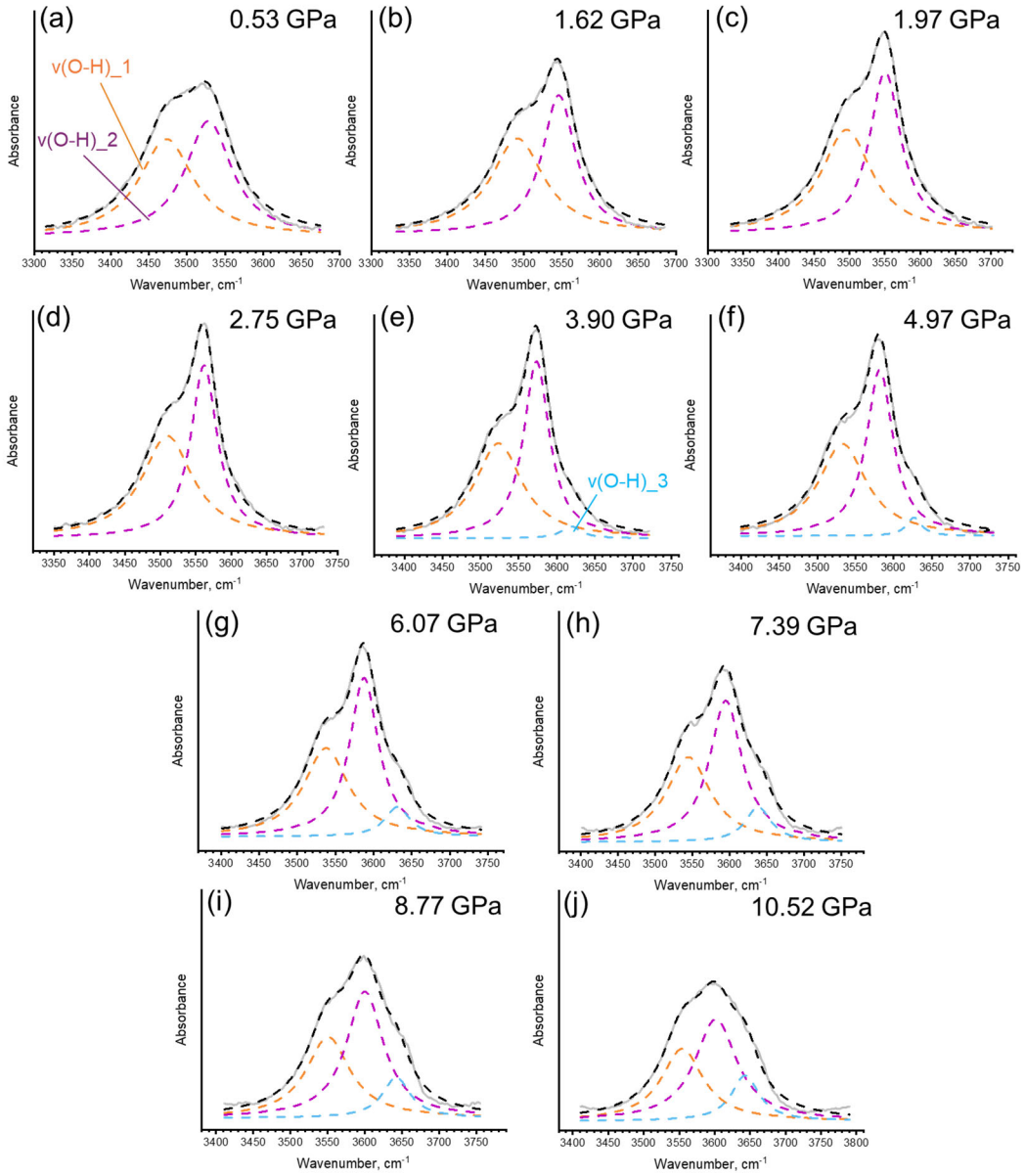

Fig. S6 Deconvolution (peak fitting) of the ν(OH) stretching band in the FTIR spectra of pre-ELM-11 at (a) 0.53 GPa, (b) 1.62 GPa, (c) 1.97 GPa, (d) 2.75 GPa, (e) 3.90 GPa, (f) 4.97 GPa, (g) 6.07 GPa, (h) 7.39 GPa, (i) 8.77 GPa, and (j) 10.52 GPa.

Table S2 The percentage of different species of the ν(OH) mode determined based on the deconvoluted areas and the goodness-of-fit parameters (adjusted R-square value, Chi-square value and residual sum of squares).

Pressure (GPa)	Percentage of Different Species			Adjusted R-Square Value	Residual Sum of Squares (10^{-2})	Chi-Square Value (10^{-5})
	ν(OH)_1 (%)	ν(OH)_2 (%)	ν(OH)_3 (%)			
0.53	49.3	50.7	-	0.996	2.31	4.15
1.62	49.1	50.9	-	0.997	1.97	3.64
1.97	49.3	50.7	-	0.999	1.01	1.78
2.75	48.8	51.2	-	0.999	1.12	1.91
3.90	46.4	50.9	2.7	0.997	1.99	3.93
4.97	46.3	50.4	3.2	0.995	3.58	6.84
6.07	41.1	50.7	8.2	0.997	2.00	3.85
7.39	39.5	50.5	10.0	0.996	2.65	4.94
8.77	37.3	50.4	12.4	0.995	2.95	5.58
10.52	34.9	49.7	15.3	0.994	3.05	5.24

*** The fitting peak type of all the peaks is Lorentz.**

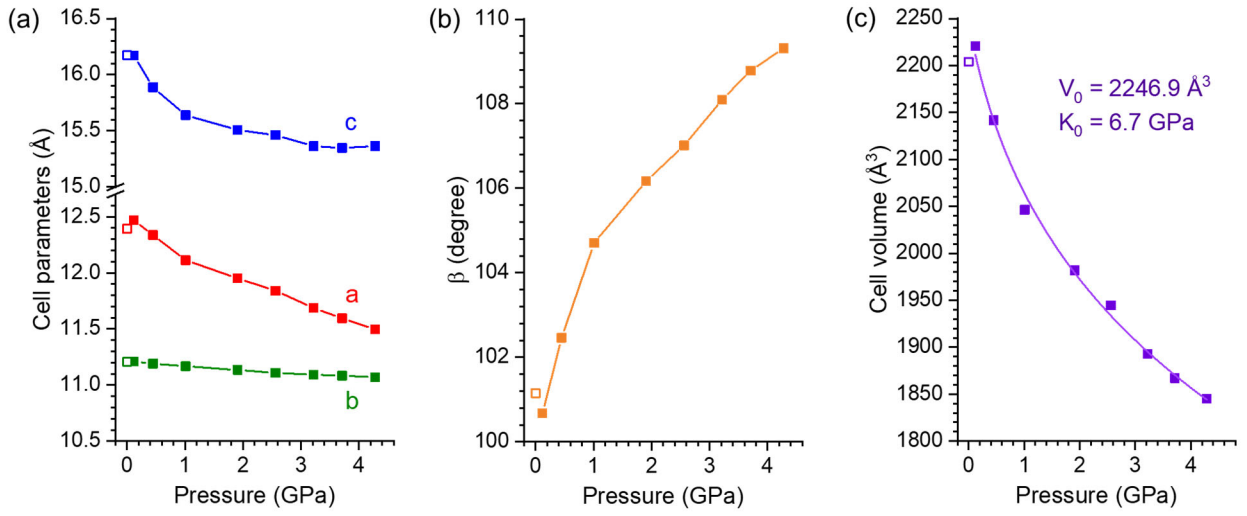

Fig. S7 Pressure dependence of (a) unit-cell parameters, (b) monoclinic angle β, and (c) unit-cell volume of ELM-11 derived from Le Bail refinement of in situ synchrotron PXRD patterns collected over 0.12–4.28 GPa. Filled squares denote compression and open squares denote recovered data after pressure release.

Table S3 The principal axes of ELM-11 at pressures ranging from 0.45 to 4.28 GPa.

	X_1			X_2			X_3		
P (GPa)	***a***	***b***	***c***	***a***	***b***	***c***	***a***	***b***	***c***
0.45	0.7332	0	0.6800	0	1	0	0.8616	0	-0.5075
1.01	0.7760	0	0.6307	0	1	0	0.8138	0	-0.5812
1.91	0.7934	0	0.6087	0	1	0	0.7898	0	-0.6134
2.56	0.8067	0	0.5909	0	1	0	0.7692	0	-0.6391
3.22	0.8170	0	0.5767	0	1	0	0.7519	0	-0.6593
3.71	0.8256	0	0.5642	0	1	0	0.7362	0	-0.6768
4.28	0.8376	0	0.5463	0	1	0	0.7127	0	-0.7014

In **Table S3**, the principal axes are expressed in terms of the crystallographic axes. Take the 1.91 GPa as an example, thus the principal axes and lattice axes are related by the matrix algebra:

$$\begin{bmatrix} X_1 \\ X_2 \\ X_3 \end{bmatrix} = \begin{bmatrix} 0.7934 & 0 & 0.6087 \\ 0 & 1 & 0 \\ 0.7898 & 0 & -0.6134 \end{bmatrix} \begin{bmatrix} a \\ b \\ c \end{bmatrix}$$

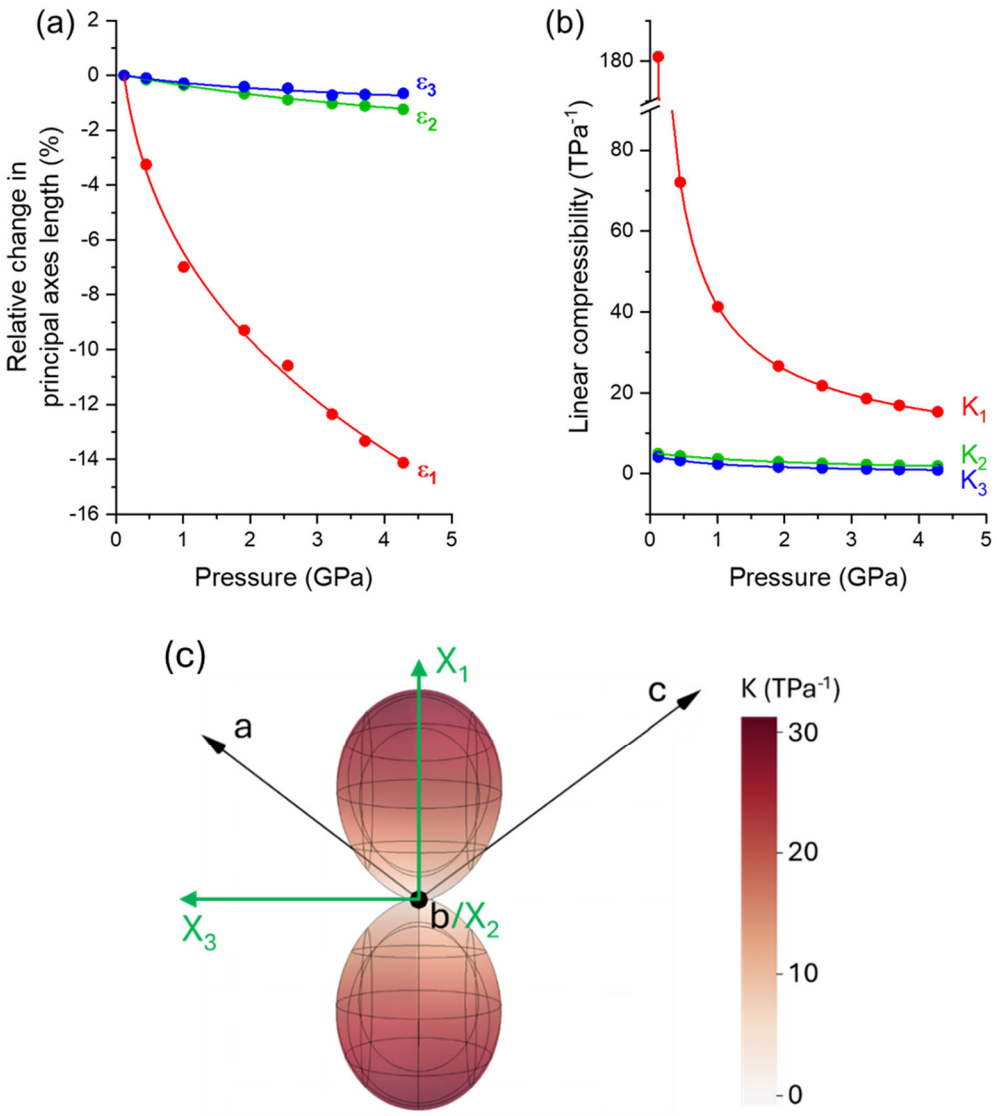

Fig. S8 (a) Relative change in length and (b) linear compressibility along the principal axes (X1–X3) of ELM-11 obtained from PASCal analysis over 0.12–4.28 GPa. (c) Linear-compressibility indicatrix at 1.91 GPa viewed along the X2 principal axis.

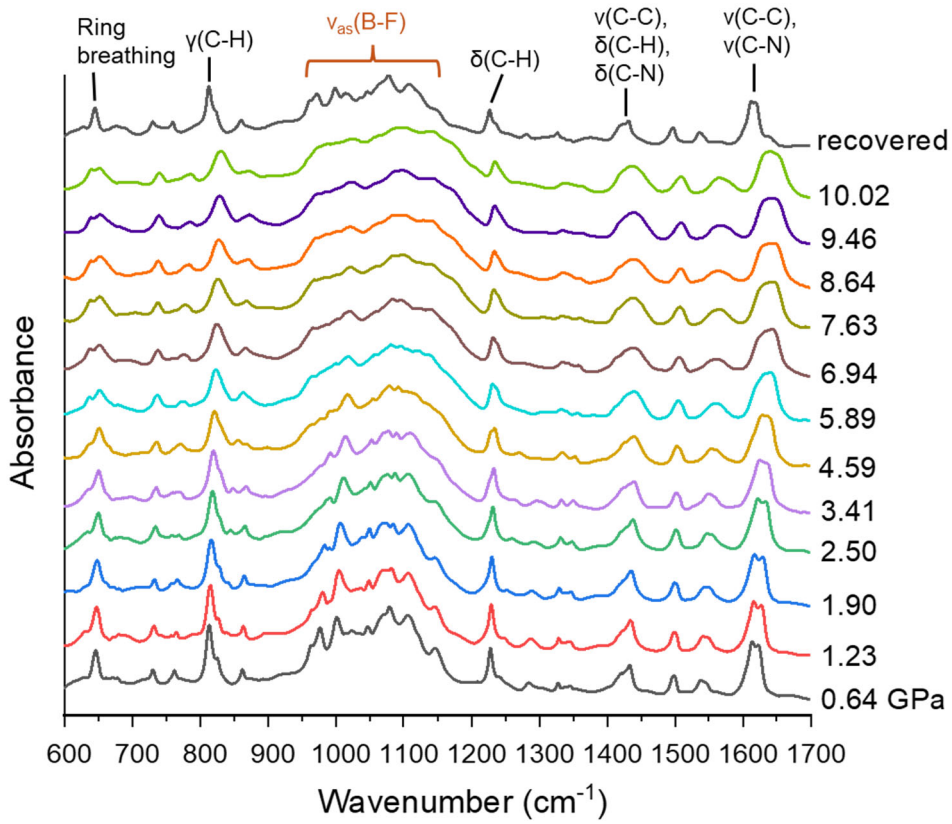

Fig. S9 Selected in situ FTIR spectra of ELM-11 collected on compression and decompression in the 600–1700 cm^{-1} range.

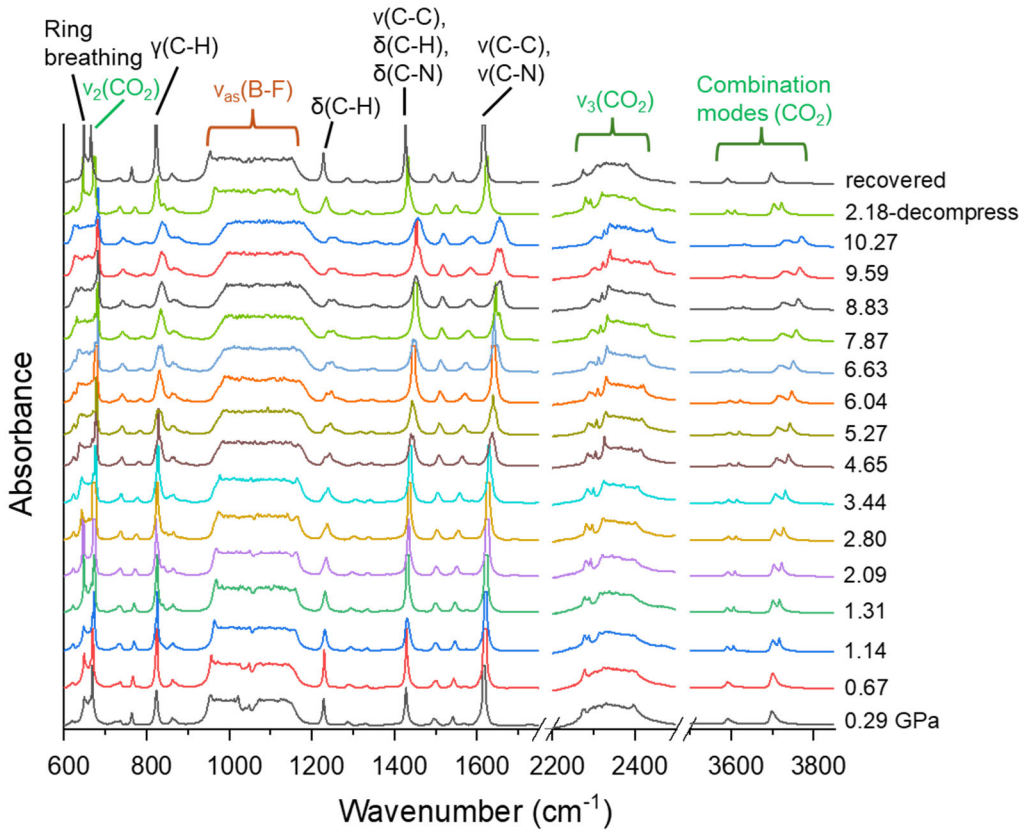

Fig. S10 Selected in situ FTIR spectra of CO_2-loaded ELM-11 collected on compression and decompression in the 600–3850 cm^{-1} range.

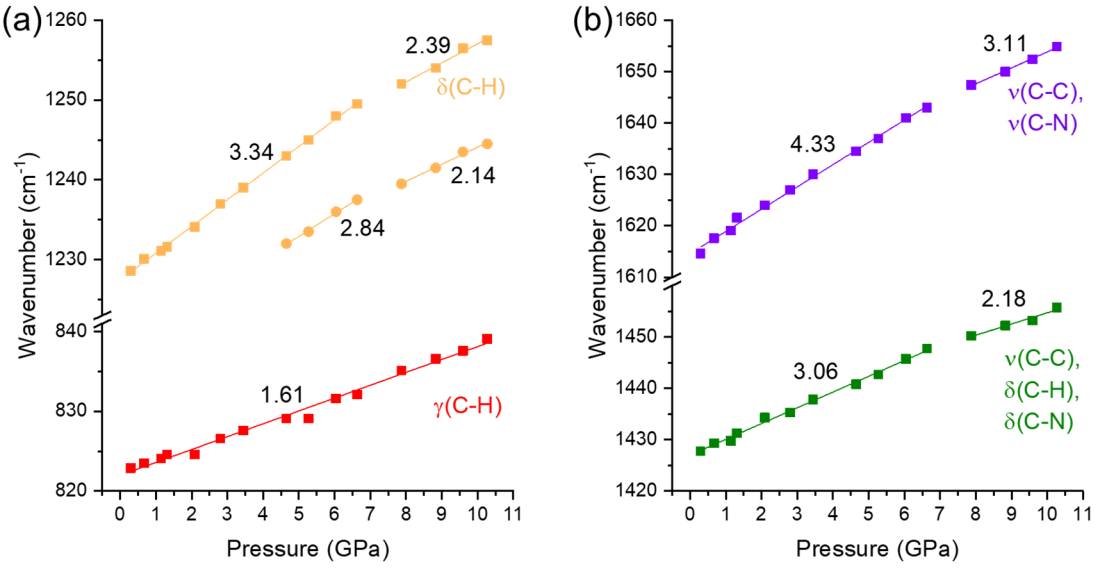

Figure S11 Pressure dependence of selected framework vibrational frequencies for CO_2-loaded ELM-11 in the (a) 820–1260 cm^{-1} and (b) 1420–1660 cm^{-1} regions (lines indicate linear fits; labelled values give pressure coefficients, dv/dP).

Table S4 The percentage of different species of the ν_3 mode of $^{13}CO_2$ determined based on the deconvoluted areas and the goodness-of-fit parameters (adjusted R-square value, Chi-square value and residual sum of squares).

Pressure (GPa)	Percentage of Different Species						Adjusted R-Square Value	Residual Sum of Squares (10^{-2})	Chi-Square Value (10^{-4})
	Solid CO_2 (%)	CO_2 inside (%)							
		Site 1	Site 2	Site 3	Site 4	Site 5			
1.14	31.4	56.1	12.5	-	-	-	0.996	0.895	2.35
2.80	28.2	8.7	63.1	-	-	-	0.994	2.15	5.36
3.44	26.4	9.5	51.5	12.6	-	-	0.998	0.438	1.09
6.63	27.7	38.1	21.0	13.2	-	-	0.997	0.535	1.05
9.59	27.5	28.5	29.1	7.7	7.2	-	0.999	0.206	0.332
10.27	27.2	17.6	28.6	6.1	16.7	3.8	0.999	0.117	0.198

*** The fitting peak type of all the peaks is Gaussian.**

References

1. A. J. Blake, S. J. Hill, P. Hubberstey and W.-S. Li, *J. Chem. Soc., Dalton Trans.*, 1997, **6**, 913-914.
2. S. Hiraide, H. Tanaka and M. T. Miyahara, *Dalton Trans.*, 2016, **45**, 4193-4202.
3. D. Jiang, A. Urakawa, M. Yulikov, T. Mallat, G. Jeschke and A. Baiker, *Chem. Eur. J.*, 2009, **15**, 12255-12262.
4. Z. Zhuang, J. Cheng, X. Wang, B. Zhao, X. Han and Y. Luo, *Spectrochim. Acta A*, 2007, **67**, 509-516.